Eur. J. Mech. B/Fluids, **17**, n° 4, 535–547, 1998

Intermittency in the closed flow between coaxial corotating disks

J. F. PINTON *, F. CHILLÀ, N. MORDANT

ABSTRACT. – We report an experimental study of the swirling flow generated in the gap between two coaxial corotating disks in an enclosed geometry, i.e. when the flow is enclosed in a cylindrical vessel. In this situation the angular momentum generated by the disk rotation tends to concentrate in a strong axial vortex. In the range of high Reynolds numbers explored, we show that two regimes exist, depending on the disk angular velocities. When they rotate at quite different speeds, we observe very intermittent fluctuations of the axial vorticity associated with quasi-periodic vortex bursting, whereas at comparable rotation rates a more stable vorticity structure is observed. We describe these regimes using global measurements; we also show, using local velocimetry, how the structure of the flow affects the small scale turbulence.© Elsevier, Paris

1. Introduction

Over the last decade, there has been a growing interest in the study of the so-called von Kármán flow between coaxial disks (Zanddberg and Dijkstra, 1987). The reason is that in a counter rotating geometry with fast rotating disks, it provides a homogeneous turbulent flow in a compact volume of space while the corotating geometry is well adapted to the study of vorticity dynamics. The counter rotating flow displays many characteristics of the turbulence observed in large wind tunnels (Maurer *et al.*, 1994; Pinton and Labbé 1994, Belin *et al.*, 1996). In addition it has allowed new measurements of quantities such as pressure fluctuations at the flow wall (Fauve *et al.*, 1993, Abry *et al.*, 1994, Cadot *et al.*, 1995) and power fluctuations: as the flow is forced with the disks rotating at constant angular velocities, the power delivered by the driving motors fluctuates in time (Labbé *et al.*, 1996a). It has also lead to the observation and study of vorticity filaments (Brachet 1990, Douady *et al.*, 1991, Cadot *et al.*, 1995, Dernoncourt *et al.*, 1997). In the corotating case, the rotation of the disks creates angular momentum and also produces a strong axial flow. Under both actions, and at large rotation rates, the vertical vorticity concentrates in a strong axial vortex. In previous studies we have shown that in the absence of lateral walls this vortex is stable, located off-axis and that it undergoes a slow precession motion (Labbé *et al.*, 1996b). We have also established that the presence of the vortex modifies the local structure of the turbulent velocity fluctuations (Chillà *et al.*, 1996). When the flow is enclosed in a cylindrical vessel (closed flow), Fauve *et al.* (1993) have noted the existence of quasi-periodic vortex bursting.

The purpose of this work is to describe further the closed corotating flow. We show that one control parameter is the ratio of the rotation rates of the disks. When they rotate at comparable speeds a strong axial vortex is formed, in addition to the turbulent background flow. When the rotation rates are quite different, the axial vortex is unstable and undergoes quasi-periodic bursting. In this regime we also describe the turbulent velocity fluctuations as a function of the distance from the rotation axis.

École Normale Supérieure de Lyon, CNRS URA 1325, 46 allée d'Italie, 69364 Lyon, France; E-mail: pinton@physique.ens-lyon.fr, fchilla@physique.ens-lyon.fr

* Correspondence and reprints

0997-7546/98/04/© Elsevier, Paris

2. Experimental set-up

2.1. Flow geometry

The coaxial corotating disks have radius R and are set a distance H apart. Cylindrical walls surround the flow volume. The experimental set-up is sketched in Figure 1. We use two different fluids, air and water.

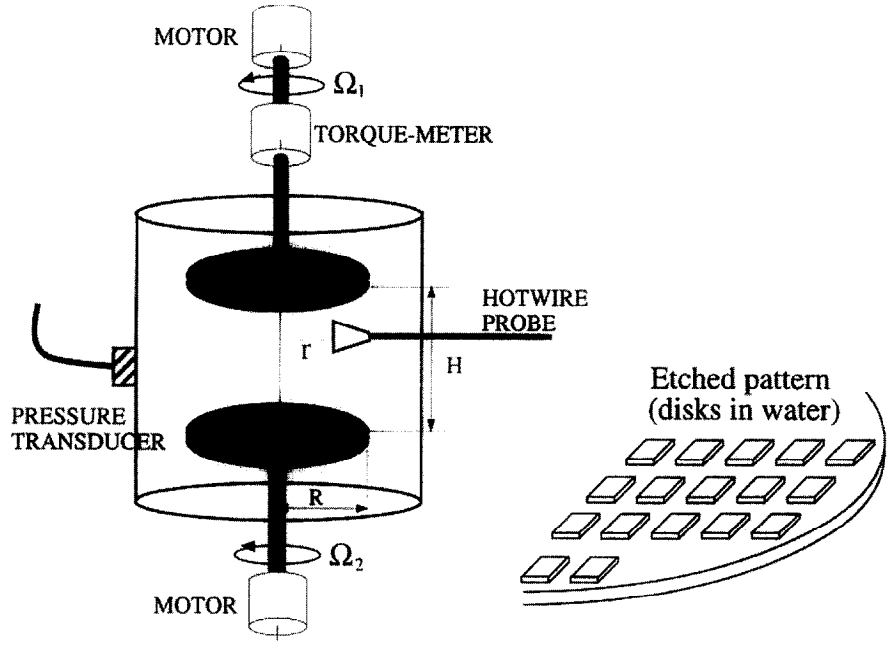

Fig. 1. – Experimental set-up. In air the disks are fitted with 8 vertical blades 2 cm high; in water the surfaces of the disks are rough, as sketched on the right of the figure.

– In the case of air, $R = 10$ cm, $H = 30$ cm. In order to increase entrainment, the disks are fitted with a set of 8 vertical blades, perpendicular to the disk surfaces, with height $h_b = 2$ cm and thickness 0.5 cm. They are driven by independent 450 watt *d.c.* motors, the rotation frequencies (Ω_1, Ω_2) of which are adjustable from 0 to 45 Hz and controlled by a feed-back loop. The flow is enclosed in a cylinder 23.2 cm in diameter. One control parameter of the flow structure is the ratio of the disk angular velocities, measured as:

$$\Psi = \frac{|\Omega_1 - \Omega_2|}{\sqrt{\Omega_1^2 + \Omega_2^2}}$$

The other control parameter is the Reynolds number, defined here as:

$$\mathrm{Re} = \frac{R^2\sqrt{\Omega_1^2 + \Omega_2^2}}{\nu}$$

(ν is the fluid kinematic viscosity). The largest value is $\mathrm{Re} \sim 10^5$.

- In the case of water, disks of radius $R = 9$ cm, $H = 20$ cm apart, are enclosed in a cylindrical container, with 19.3 cm inner diameter and 23.8 cm height. The disk surfaces have an etched pattern in the form of squares 2 mm high and 5 mm wide, so that the rugosity is always larger than the boundary layer; entrainment is then equivalent to using blades (Mordant *et al.*, 1997). The temperature is kept constant with a regulated water circulation. The disks are rotated independently by two Parvex-Alsthom RS420 motors at controlled rotation frequencies in the range [0,40] Hz. The Reynolds numbers achieved are greater than 10^6.

2.2. Measurements

- Visualization is performed in water using micro air bubbles and taking advantage of the fact that they migrate towards low pressure regions which have been associated with vorticity concentrations (Brachet 1990, Douady *et al.*, 1991). The visualization is performed by scattering a blue argon laser light sheet, observed at 90 degrees. With this setup, quantitative measurements are also possible by imaging and recording the scattered light intensity using a photodiode (active equal to 3 mm).
- Pressure measurements in water are done with a 5 mm $PCBH112A21$ piezoelectric transducer, mounted flush with the lateral wall, in the mid-plane between the disks. It is acceleration-compensated and has a low frequency cut-off at -3 dB equal to 50 mHz; its rise-time is 1 ms. Pressure fluctuations in air are measured by a piezoelectric transducer $PCB103A02$, also mounted flush with the lateral wall and in the mid-plane. Its active diameter is 2.1 mm, its low frequency cut-off at -5 % is 0.05 Hz and its rise-time is 25 μs.
- Local velocity measurements are performed in air using a TSI IFA100 constant temperature anemometer and a TSI 1260A-10 subminiature hot-film probe with a sensing element 10 μm thick and 0.5 mm long. The position of the probe is adjustable.

3. Global characterization and mean flow structure

The existence of two different flow regimes is observed in global measurements such as the pressure at the lateral wall. We have measured it with one disk kept at a fixed rotation rate Ω_1 while the speed of the other disk $-\Omega_2$, rotating in the same direction – is varied. The corresponding low frequency part of the pressure spectra are shown as a contour plot in Figure 2(a). When $\Omega_2 \sim \Omega_1$, that is then $\Psi \sim 0$, the spectrum has only one broad component (plus harmonics) at the rotation frequency of the disks – see Figure 2(b). When $\Omega_2 \gg \Omega_1$, i.e. $\Psi \sim 1$, more frequency lines are observed in addition to those at the rotation frequencies of each disks:

(i) a peak at $f_m \sim \frac{1}{2}(\Omega_1 + \Omega_2)$, i.e. corresponding to the mean rotation rate imparted by the disks, and,
(ii) a broad low frequency peak at $f_i < 1$ Hz – see figure 2(c) – which indicates a quasiperiodic evolution of the flow.

Note that the flow has a developed turbulence at small scales, so that the higher end of the pressure spectra show $-7/3$ scalling regions, as expected at such high Reynolds number – we will discuss small scale turbulence features in section 4.2; for the moment we are only concerned with the slow evolution of the flow. The pressure measurements indicate a motion with a characteristic frequency corresponding to the flow mean rotation rate, with a superimposed quasi-periodic slow evolution when the disks are operated at quite different speeds.

To confirm these observations we have used flow visualization in the experiment using water as the working fluid, by the addition of tiny air bubbles. Figure 3 sketches the imaging technique; the laser light sheet can either contain the rotation axis or be perpendicular to it. This arrangement allows the visualization of the overall structure and of the cross section of the axial vortices. The pictures in Figure 3 (taken from long video recordings) illustrate the different regimes:

(i) pictures 3 (a, b, c) are taken in the $\Psi \sim 0$ regime. In the axial cut -3 (a) – one observes a concentration of bubbles in the center and in a thinner cylindrical layer at about 4 cm from the rotation axis. This indicates the presence of a strong vortex centered on the rotation axis, but also of additional off-axis

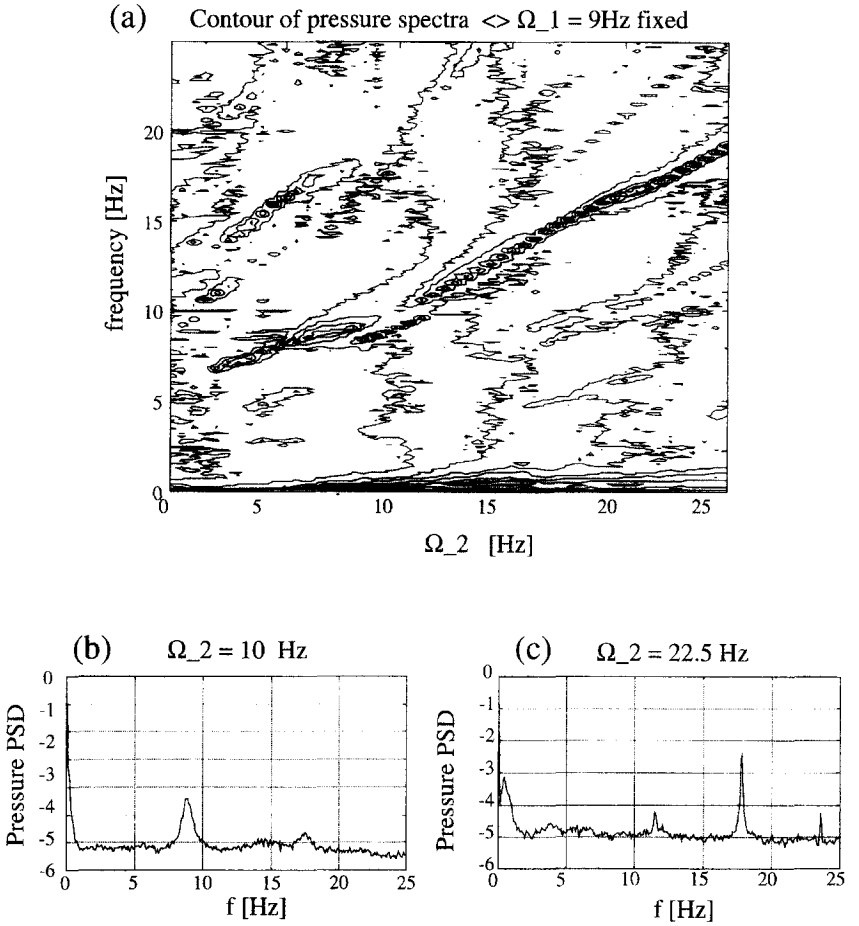

Fig. 2. – Pressure measurements at the lateral wall, in the mid-plane. One disk is kept at constant rotation rate $\Omega_1 = 9$ Hz, while the speed of the other disk is varied from 0.5 Hz to 27.5 Hz. (a) Contour plot of the low frequency part of the pressure spectra; (b) individual spectrum in semi-log coordinates for $\Omega_2 = \Omega_1$; (c) case $\Omega_2 = 22.5$ Hz. The working fluid is water, but an identical behavior is observed in the set-up using air.

vortices. The structure of this axial vorticity is revealed by the cross-sections in pictures 3(b, c): there are individual 'satellite' vortices that rotate around the central one and have a more complex dynamic. We have observed between 1 and 3 off-axis vortices depending on the mean rotation rate. On a video recording, we find that this pattern is stable in the sense that while it displays rapid fluctuations due to the turbulence of the flow, the slow and large scale features of the pattern remain unchanged.

(ii) In situations where $\Psi \sim 1$, the mean flow pattern is unstable with a quasi-periodic evolution between the state shown in Figure 3(d) where a strong axial vortex is formed and the state of figure 3(e) where the flow is completely disorganized. Picture 3(f) shows a cross section of the flow in the phase when the axial vortex is reforming.

The above statements are made more quantitative with the photodiode measurements of the scattered light intensity in the mid-plane and on the rotation axis with the light sheet set to produce an axial cut).

For $\Psi \sim 0$, one observes an irregular signal – Figure 4(a) – which has gaussian fluctuations, Figure 4(b) – and no characteristic frequency other than the mean flow rotation rate at $\Omega_1 \sim \Omega_2$ – see Figure 4(c).

On the other hand, when $\Psi \sim 1$, the light intensity signal is very asymmetric, as shown in Figure 5(a) and emphasized in the corresponding histogram in Figure 5(b). Very high bubble concentrations are detected

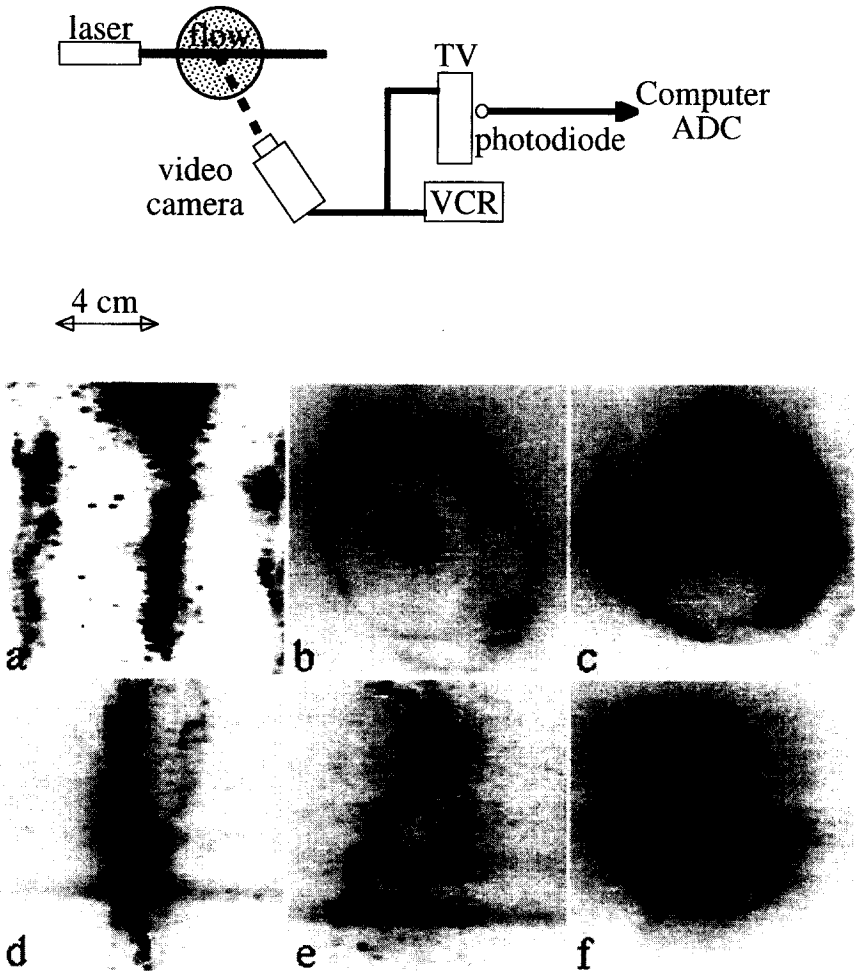

Fig. 3. – Sketch of visualization technique and measurement method, in water. (a, b, c): pictures at $\Omega_1 = \Omega_2 = 15$ Hz; (a): axial cut, (b, c): cross sections. (d, e, f): $\Omega_1 = 10$ Hz, $\Omega_2 = 22.5$ Hz; (d, e): axial cuts, (f): cross section.

at regular intervals as can be observed in Figure 5(c) and on the spectrum of light intensity in Figure 5(d). The characteristic frequency is equal to 0.7 Hz, identical to the very low frequency peak observed in the pressure spectrum.

Finally, we have measured the mean velocity in the mid-plane, as a function of the distance from the rotation axis, using a hotwire probe. In these flows the average radial velocities are much smaller than the azimuthal and vertical ones (away from the driving disks), so that when the wire is positioned vertically it essentially probes the azimuthal velocity, and when it is positioned horizontally, it essentially probes the vertical velocity.

(i) for $\Psi \sim 0$ figure 6(a), the azimuthal velocity ressembles that of a Rankine vortex, with a core region where v_θ increases almost linearly with the distance to the rotation axis. Indeed, if ones computes dv_θ/dr in this core region, one finds the rotation rate Ω of the disks, that is the mean angular velocity of the flow. We also note that the off-axis vortices are located close to the point where the vertical velocity is maximum.

(ii) the situation for $\Psi \sim 1$ figure 6(b), is quite different. The vertical velocity on the rotation axis is very high, of the order of the disk rim velocity, and drops rapidly. It defines a core region, where one also observes that the average azimuthal velocity is almost constant. Recalling $v_\theta = rd\theta/dt$, it indicates very rapid rotation rates as ones gets closer to the vortex axis. This core is surrounded by a region of very

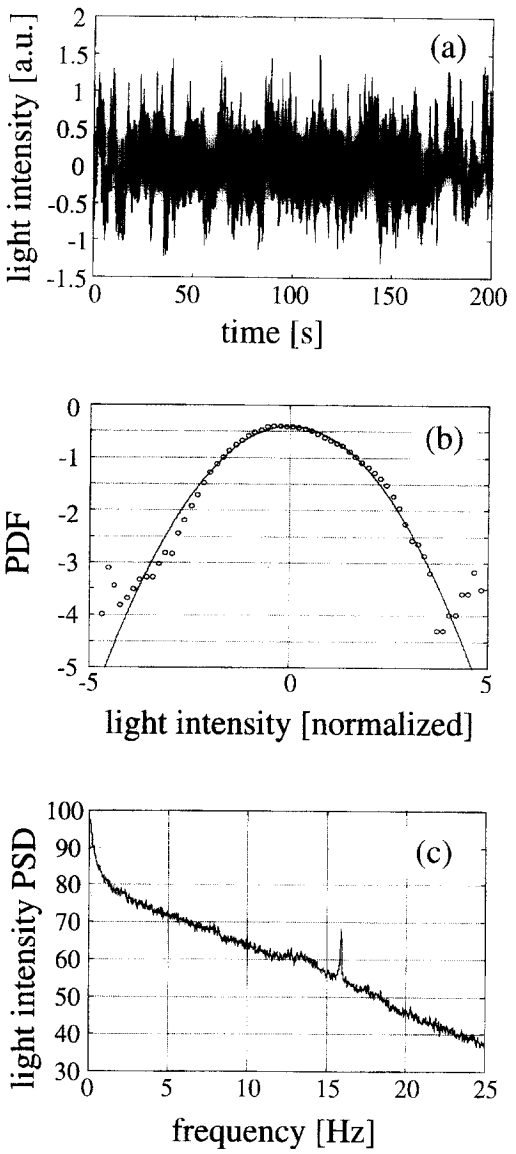

Fig. 4. – Measurement of light intensity on the image of flow, on the rotation axis and in the mid-plane. The disks rotate at equal rates $\Omega_1 = \Omega_2 = 16$ Hz. (a) time recording of the light intensity; (b) corresponding histogram and Gaussian fit; (c) spectrum of light fluctuations.

high differential rotation: in the case of the figure ($\Omega_1 = 40$ Hz, $\Omega_2 = 12$ Hz) the tangential velocity increases at the rate of 10 m/s per cm!

The picture for the large scale flow that we get from the above measurements is the following:

(i) in the regime where the disks rotate at comparable speeds $\Psi \sim 0$, a rather *stable* axial vorticity distribution vortex is formed. At large rotation rates one observes a stable central vortex surrounded by a varying number of 'satellite' vortices (e.g. *see* Figure 3(b) and 3(c)) which have a complex dynamic of formation and merging. The visualization also shows that at slow rotation rates (< 10 Hz in the water experiment), the 'satellite' vortices only are present and the central vortex is no longer observed.

(ii) when the rotation rate of the disks are quite different $\Psi \sim 1$, the flow is very unstable. An axial vortex is formed and undergoes violent bursting – for instance the photograph 3(d) shows the vortex at its peak

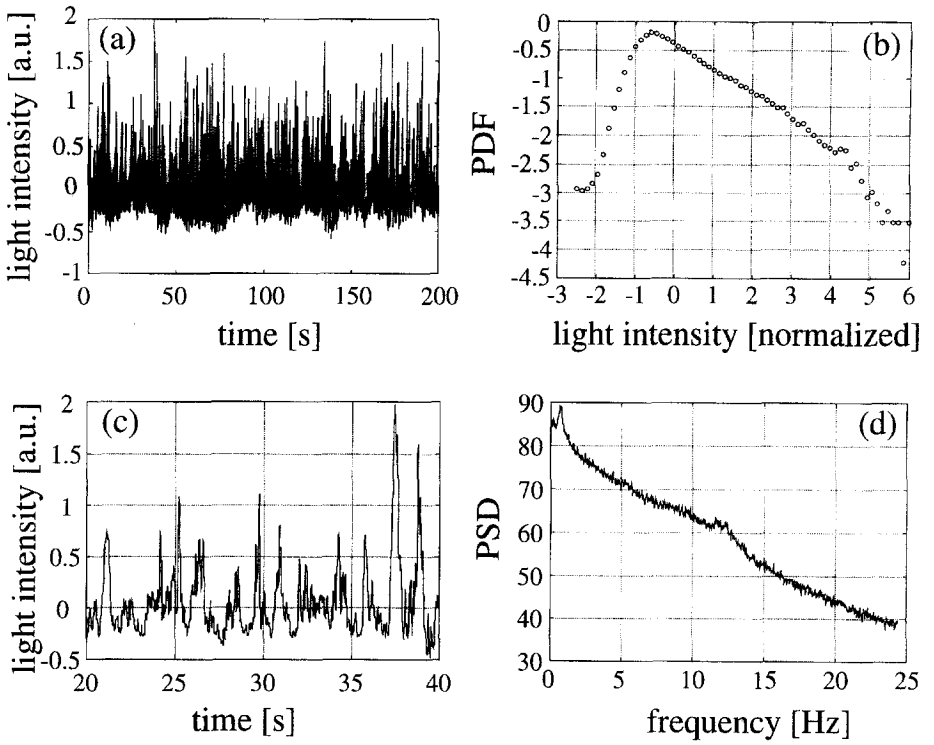

Fig. 5. – Measurement of light intensity on the image of flow, on the rotation axis and in the mid-plane. The disks rotate at equal rates $\Omega_1 = 8$ Hz, $\Omega_2 = 20$ Hz. (a) time recording of the light intensity; (b) corresponding histogram; (c) detail of the light fluctuations – note the $\tau \sim 1$ second period; (d) corresponding spectrum – note the peak at $f \sim 1/\tau$.

intensity whereas 3(e) is taken at the onset of bursting. The sequence is quasiperiodic with a very slow period compared to the average disk rotation rates – typically one order of magnitude slower.

These regimes of the corotating von Kármán flow are far from being completely understood, and are the subject of further investigations. In the next section we show in the unstable regime that the large scale dynamics influence the properties of the flow at small scales.

4. The unstable vortex regime

4.1. Study of the vortex breakdown

We first note that this is the common situation since the axial vortex is stable only in the range $\Psi < 0.2$. This relatively small stability domain might be linked to the observation (Couder *et al.*, 1997) that the formation of a vortex under axial stretching is a two step process: first the axial vorticity is concentrated by the initial velocity gradients and then, once the vortex is formed, it reacts on the flow. The final vorticity profile is then the result of an equilibrium between the action of the imposed stretching and of the flow induced by the axial vortex. As this is achieved over times of the order of the vortex rotation period ω^{-1}, a possibility when the disks rotate at too different speeds is that such equilibrium cannot be reached, leading to the unstable dynamics.

To investigate the bursting phenomenon we have made axial velocity measurements with a hotwire probe located on the axis of rotation, in the mid-plane. A typical long time recording is shown in Figure 7(a) for $\Omega_1 = 40$ Hz and $\Omega_1 = 12$ Hz, in air: the velocity is very asymmetric with strong spikes towards low values. Our observation is that these low velocity sharp events have the same characteristics as the vortex bursting as

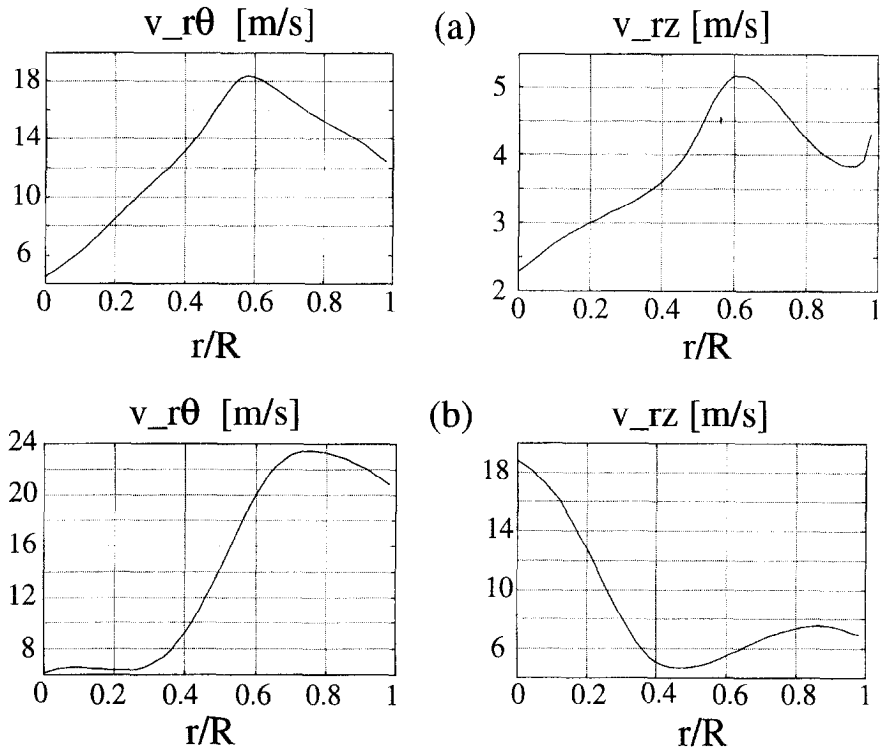

Fig. 6. – Mean velocity profiles measured with a single hot wire probe, in air. When the probe is set vertically it measures $v_{r\theta} = \sqrt{v_r^2 + v_\theta^2}$, while in the horizontal position it measures $v_{rz} = \sqrt{v_r^2 + v_z^2}$. (a) $\Omega_1 = \Omega_2 = 30$ Hz; (b) $\Omega_1 = \Omega_2 = 40$ Hz, $\Omega_2 = 12$ Hz.

recorded by the light intensity measurements on the rotation axis. Both signals have histograms with enhanced tails on one side. In addition, the mean waiting times between sharp velocity drops (e.g. $u/U < 0.2$) is equal to the period of formation of the strong axial vortex. This is also observed in the velocity spectrum which has a peak at the same very low frequency (Figure 7(b)), peak indicated by an arrow, at $f = 1.8$ Hz) as present on the pressure and light intensity measurements (Figure 5(d)). We thus identify the occurrence of a strong drop in the axial velocity with the bursting of the axial vortex; this is in agreement with traditional acronautical studies on vortex breakdown (Hall 1972, Leibovich 1978). We have noted that the average duration of the sharp velocity drops is very small – about 10 ms, Figure 7(c). The breakdown of the vortex itself, as characterized by the decrease of the light intensity as in Figure 5(c), takes place in a time scale of the order of the mean rotation rate.

4.2. Turbulences features

We now turn to the analysis of the turbulent velocity fluctuations as measured by a hotwire probe, in the mid-plane and at a variable distance r from the rotation axis. As will be demonstrated, there is a strong anisotropy in the velocity field in this flow. For each position r, we study the small scale properties of $v_{r\theta} = \sqrt{v_r^2 + v_\theta^2}$ (wire positioned parallel to the rotation axis) and of $v_{rz} = \sqrt{v_r^2 + v_z^2}$ (wire positioned perpendicular to the rotation axis). We compute the power spectral density of the velocity signal, and study the statistical characteristics of the absolute value of the velocity increments, *via* the moments $F_p(\tau)$ and the scaling exponents ζ_p defined as:

$$F_p(\tau) = \langle |v(x+\tau) - v(x)|^p \rangle_x \propto \tau^{\zeta_p}.$$

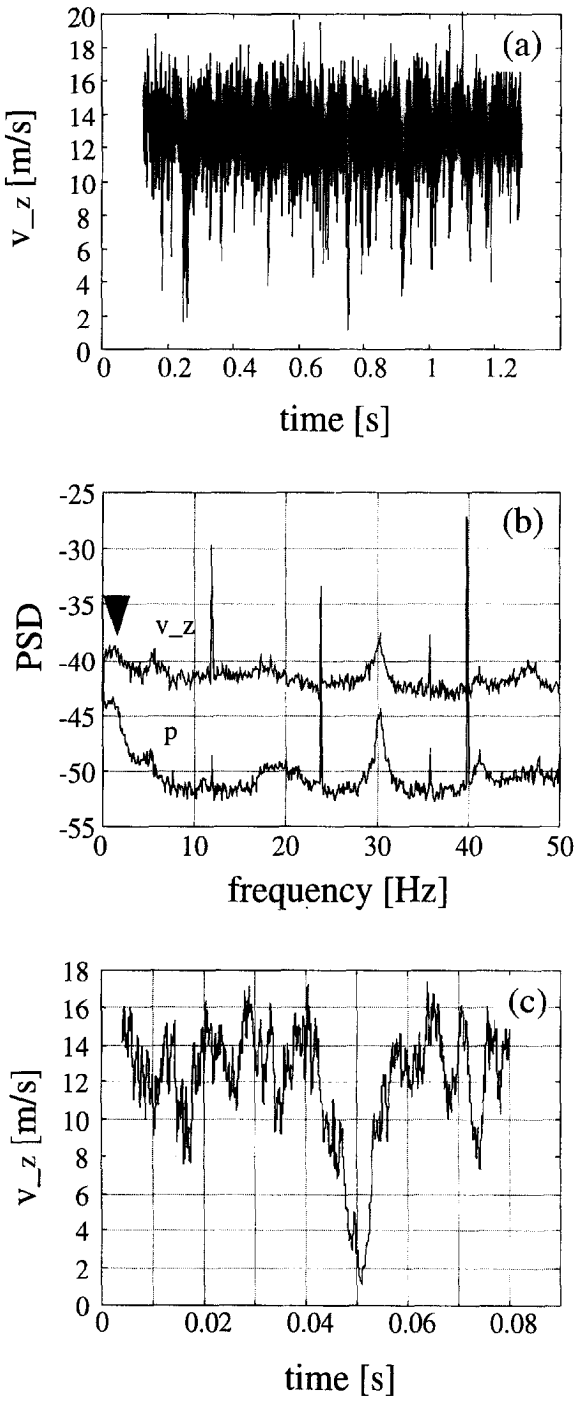

Fig. 7. – Local measurement of the axial velocity in air with a hot wire probe located on the axis of rotation. (a) evolution in time of the velocity signal; (b) corresponding power spectrum (upper curve), compared to the spectrum at the wall (lower curve). The peak indicated by an arrow at $f = 1.8$ Hz corresponds to the periodic bursting of the central vortex; (c) detail of a velocity drop.

The exponents are computed relative to the 3rd order exponent ($\xi_p = \zeta_p/\zeta_3$) using the "extended self-similarity" (ESS) ansatz (Benzi *et al.*, 1995).

Figure 8 shows the $v_{r\theta}$ turbulence characteristics in air when the distance from the rotation axis is varied, for $\Omega_1 = 40$ Hz and $\Omega_2 = 12$ Hz. We observe three different regions:

- *region* $(I\theta)$ close to the vortex core $(\tau/R < 0.3)$: the velocity power spectra show a scaling region, but with a slope that decreases continuously as one gets nearer to the vortex core – Figure 8(a). For instance, at $\tau/R = 0.05$ it is equal to -1.2, consistent with the $F_3(\tau) \propto \tau^{0.5}$ behavior observed in Figure 8(b). In this region, the relative structure function exponents have very intermittent values, as shown in Figure 8(c).
- *region* $(II\theta)$ corresponds to the interval $(0.4 < \tau/R < 0.7)$ is characterized by the presence of a large differential rotation in the radial direction in Figure 6(b). In this region, the velocity power spectra exhibit

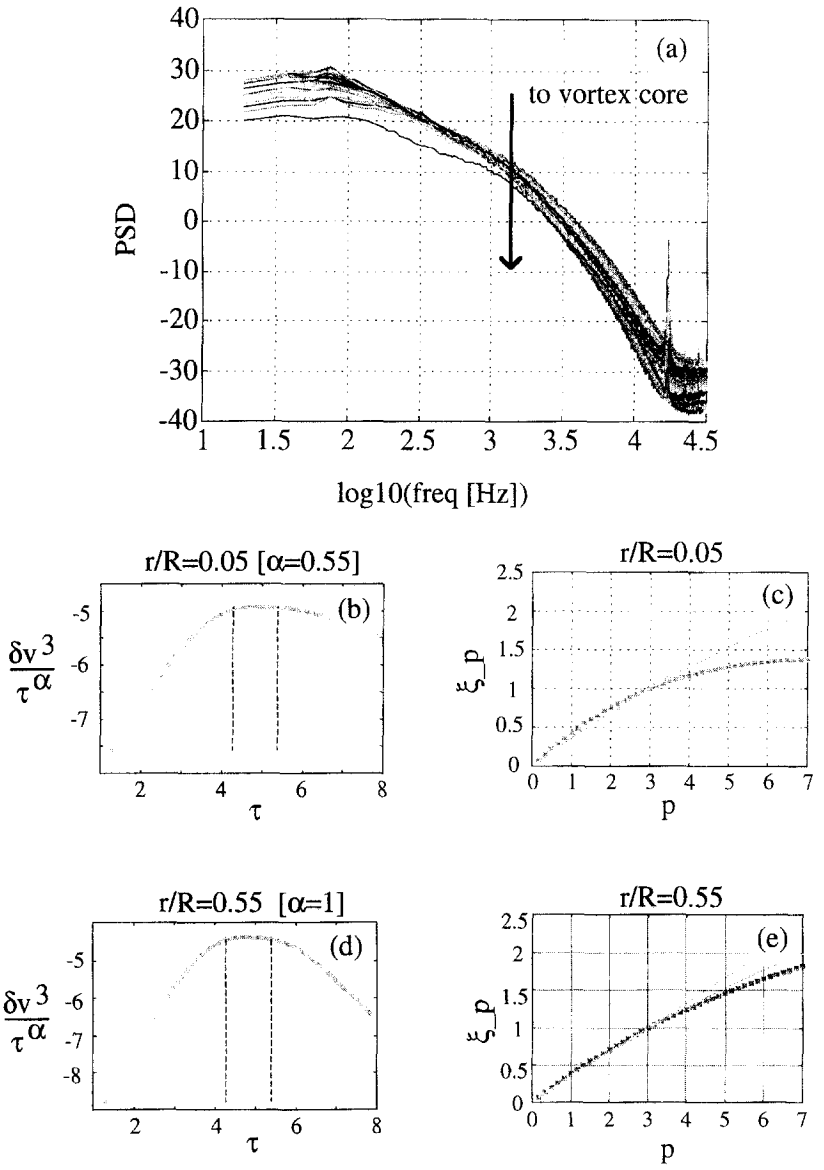

Fig. 8. – Local measurement, in air, of the $v_{r\theta}$ velocity component, as a function of the distance from the rotation axis, in the mid plane. The statistics are computed from series of 2^{20} data points, sampled at a 78125 Hz. (a) Velocity power spectra. (b, d) 3rd order structure function in the core region $(I\theta \equiv \tau/R < 0.3)$; the dotted lines limit the region used for the scaling exponent calculations; (c, e) corresponding relative exponents $\xi_p = \zeta_p/\zeta_3$, from $p = 1/6$ to 7 in steps of $1/6$; the solid straight line is the Kolmogorov K41 $\xi_p = p/3$ prediction and the dotted lines are the values observed in isotopic homogeneous turbulence.

a clear Kolmogorov $-5/3$ scaling in the range of scales where $F_3(\tau) \propto \tau$ as shown in Figure 8(d). However, the relative exponents ξ_p have values that, compared to region $(I\theta)$ are closer to those observed in homogeneous, isotropic turbulence (Arnéodo *et al.*, 1996).

- *region* $(III\theta)$ close to the lateral wall $(\tau/R < 0.8)$: the spectra are very rounded and we do not observe a clear scaling behavior.

The behavior of the axial component reveal the flow anisotropy at all scales. Indeed, Figure 9 shows the same analysis for v_z measured at the same distance from the rotation axis. The velocity power spectra display scaling regions now with increasing slopes as one gets closer to the vortex core – Figure 9(a). Two regions only can clearly identified:

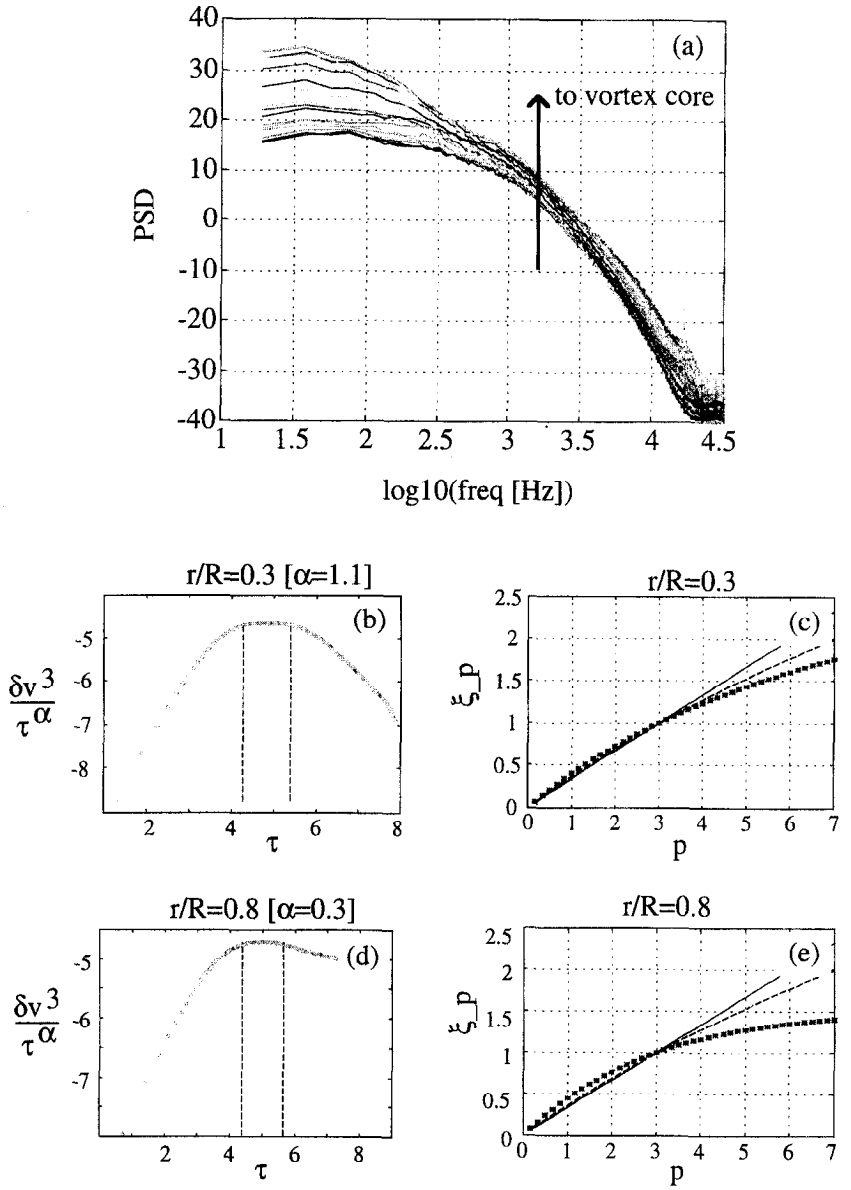

Fig. 9. – Same as figure 9, for the $v_{\tau z}$ velocity component.

- *region* (Iz) close to the vortex core $(\tau/R < 0.35)$: the velocity spectrum shows roughly one decade of Kolmogorov $-5/3$ scaling in a domain where $F_3(\tau)$ scales as τ Figure 9(b). The relative exponents ξ_p have values consistent with those observed in isotropic, homogeneous turbulence – Figure 9(c).
- *region* (IIz) outside the vortex cote $(\tau/R > 0.5)$: the slopes of the velocity spectra decrease towards -1 and the intermittency increases as evidenced by the curvature of the relative exponent $\xi_p(p)$, in a fashion that is similar to region $(I\theta)$ – see figures 9(d, e).

5. Conclusion

Global measurements in the closed flow between coaxial corotating disks lead to the identification of two regimes, as the ratio of the rotation speeds of the disks is varied. When $\Psi \sim 1$, violent vortex bursting is observed, whose dynamics seem to be a result of the existence of differential rotation, in agreement with a mechanism recently proposed for the instability of finite length vortices (D. Samuels 1997).

The modifications of the flow geometry and dynamics in this unstable regime also affect the statistical properties of the turbulent fluctuations. The flow is strongly anisotropic down to the smallest scales. A power law scaling in the spectrum is observed and the ESS ansatz allows the measurement of structure function exponents. There is no evidence that a universal behavior is reached that could describe the statistical properties of the turbulent fluctuations. As the distance from the intermittent structure decreases, the azimuthal and axial velocity components behave differently, with the azimuthal one becoming more intermittent. How this is related to the large scale structure of the flow and to the vortex bursting events is yet unclear. Further analysis based on conditional averaging techniques is underway.

Acknowledgements. – We would like to thank Franck Vittoz and Marc Moulin for continuous help with the experimental setup and Mathieu Baudry for his participation in some of the measurements reported here, as part of his graduate summer project.

REFERENCES

ABRY P., FAUVE S., FLANDRIN P., LAROCHE C., 1994, Analysis of pressure fluctuations in swirling turbulent flows, *J. Phys. II France* **4**, 725-733.

ARNÉODO A. *et al.*, 1996, Structure functions in turbulence in various flow configurations at Reynolds numbers between 30 and 5000, using Extended Self Similarity, *Europhys. Lett.*, **34**, 411-416.

BELIN F., MAURER J., TABELING P., WILLAIME H., 1996, Observation of intense filaments in fully developed turbulence, *J. Phys. II France,* **6**, 573-583.

BENZI R., CILIBERTO S., BAUDET C., RUIZ-CHAVARRIA G., 1995, On the scalling of three dimensional homogeneous isotropic turbulence, *Physica D,* **80**, 385-398.

BRACHET M., 1990, Geometrie des structures à petite échelle dans le vortex de Taylor-Green, *C. R. Acad. Sci. Paris,* **311**,(II), 775-780.

CADOT O., DOUADY S., COUDER Y., 1995, Characterization of the low pressure filaments in a three dimensional turbulent shear flow, *Phys. Fluids* **A7**, 630-646.

CHILLÀ F., PINTON J.-F., LABBÉ R., 1996, On the influence of a large scale coherent vortex on the turbulent cascade, *Europhys. Lett.*, **35**, 271-276.

COUDER Y., ANDREOTTI B., DOUADY S., 1997, The formation of vorticity filaments; experiments on the interaction of vorticity and strain, invited lecture, Euromech 364, Carry-le-Rouet, June 1997.

DERNONCOURT B., PINTON J.-F., FAUVE S., 1998, Experimental study of vorticity filaments in a turbulent swirling flow, *Physica D*, in press.

DOUADY S., COUDER Y., BRACHET M.-E., 1991, Direct observation of the intermittency of intense vorticity filaments in turbulence, *Phys. Rev. Lett.*, **67**, 983-986.

FAUVE S., LAROCHE C., CASTAING B., 1993, Pressure fluctuations in swirling turbulent flows, *J. Phys. II France*, **3**, 271-278.

HALL M. G., 1972, Vortex breakdown, *Ann. Rev. Fluid Mech.*, **4**, 195-218.

LEIBOVICH S., 1978, The structure of vortex breakdown, *Ann. Rev. Fluid Mech.*, **10**, 221-246.

LABBÉ R., PINTON J.-F., FAUVE S., 1996a, Power fluctuations in turbulent swirling flows, *J. Phys. II France*, **6**, 1099-1110.

LABBÉ R., PINTON J.-F., FAUVE S., 1996b, Study of the von Kármán flow between coaxial corotating disks, *Phys Fluids,* **8**, 914-922.

MAURER J., TABELING P., ZOCCHI G., 1994, Statistics of turbulence between two counter rotating disks in low temperature helium gas, *Europhys. Lett.,* **26**, 31-36.

MORDANT N., PINTON J.-F., CHILLÀ F., 1997, Characterization of turbulence in a closed flow, *J. Phys. II France,* **7**, 1729-1742.

PINTON J.-F., LABBÉ R., 1994, Correction to the Taylor hypothesis in swirling flows, *J. Phys. II,* **4**, 1461-1468.

SAMUELS D., 1997, A finite length instability of vortex tubes, This volume.

ZANDBERG P. J., DIJKSTRA D., 1987, Von Kármán swirling flows, *Ann. Rev. Fluid Mech.,* **19**, 465-491.

(Received 17 July 1997,
revised 12 December 1997,
accepted 17 February 1998)